Human T2D-Associated Gene *IMP2/IGF2BP2* Promotes the Commitment of Mesenchymal Stem Cells Into Adipogenic Lineage

Laura Regué,[1,2,3] William Wang,[4,5] Fei Ji,[1,3] Joseph Avruch,[1,2,3] Hua Wang,[4,5] and Ning Dai[1,2,3]

Diabetes 2023;72:33–44 | https://doi.org/10.2337/db21-1087

Excessive adiposity is the main cause of obesity and type two diabetes (T2D). Variants in human *IMP2/IGF2BP2* gene are associated with increased risk of T2D. However, little is known about its role in adipogenesis and in insulin resistance. Here, we investigate the function of IMP2 during adipocyte development. Mice with Imp2 deletion in mesenchymal stem cells (MSC) are resistant to diet-induced obesity without glucose and insulin tolerance affected. Imp2 is essential for the early commitment of adipocyte-derived stem cells (ADSC) into preadipocytes, but the deletion of Imp2 in MSC is not required for the proliferation and terminal differentiation of committed preadipocytes. Mechanistically, Imp2 binds Wnt receptor *Fzd8* mRNA and promotes its degradation by recruiting CCR4-NOT deadenylase complex in an mTOR-dependent manner. Our data demonstrate that Imp2 is required for maintaining white adipose tissue homeostasis through controlling mRNA stability in ADSC. However, the contribution of IMP2 to insulin resistance, a main risk of T2D, is not evident.

Expansion of white adipose mass through adipogenesis is the key contributor of obesity. The development of white adipose depots can be divided into two stages: *1*) early commitment, which involves differentiation of ADSC ($CD24^+$) into preadipocytes ($CD24^-$), followed by *2*) terminal differentiation of committed preadipocytes into mature adipocytes (1). The nutrient sensing mTOR pathway is essential for both processes to promote adipogenesis (2). On the other side, it is well-known that Wnt/β-catenin signaling restrains adipogenesis by preventing both the commitment of ADSC into preadipocytes and their final differentiation (3). However, the connection of the two pathway is poorly understood.

The insulin-like growth factor 2 (IGF2) mRNA binding proteins (IMPs or IGF2BPs) are a conserved family of single-stranded RNA binding proteins and composed of six canonical RNA binding domains, including two RNA recognition motif (RRM) domains and four K homology (KH) domains. IMPs participate in the splicing, transport, translation, and stabilization of a wide variety of RNAs in a transcript- and tissue-specific manner (4). Recently, IMPs were identified as readers of N^6-methyladenosine (m^6A), the most abundant modification of eukaryotic RNAs. They are capable of recognizing thousands of RNAs through the consensus sequence GG(m^6A)C (5). IMPs are onco-fetal proteins that are essential for stem cell proliferation and differentiation during embryonic development (6) as well as cancer progress (7). In addition, IMPs are direct substrates of mTOR, and the phosphorylation of IMPs by mTOR regulates the RNA life cycle in response to nutrients (8,9).

Genome-wide association studies have identified single nucleotide polymorphisms (SNPs) in the second intron of the human *IMP2* gene to be associated with increased risk for type 2 diabetes (T2D) in many populations (10–12). Follow-up human genetic studies further demonstrated that the association of *IMP2* intronic SNPs is affected through modification of the expression of *IMP2* gene itself instead of neighboring genes in pancreatic islets, supporting the idea that IMP2 is directly involved in T2D pathophysiology (13,14).

[1]Department of Molecular Biology, Massachusetts General Hospital, Boston, MA
[2]Diabetes Unit of the Medical Services, Massachusetts General Hospital, Boston, MA
[3]Department of Medicine, Harvard Medical School, Boston, MA
[4]The Lundquist Institute, Torrance, CA
[5]David Geffen School of Medicine, University of California, Los Angeles, Los Angeles, CA

Corresponding authors: Ning Dai, ndai78@gmail.com, and Hua Wang, hua.wang@lundquist.org

Received 6 December 2021 and accepted 6 October 2022

This article contains supplementary material online at https://doi.org/10.2337/figshare.21298485.

For ascertainment of whether IMP2 participates in the regulation of nutrient metabolism, mice lacking Imp2 were generated and characterized (15). Imp2 knockout mice exhibit a normal birth size and body weight similar to that of control littermates until weaning. However, they gain less weight on normal chow diet (NCD) or on a high-fat diet (HFD), due to slower accumulation of both lean and fat mass. The lower fat mass of Imp2 null mice is especially marked on HFD and is accompanied by considerably better glucose tolerance and insulin sensitivity (15). The beneficial but complicated phenotypes of Imp2 null mice prohibit further understanding of IMP2 functions in individual metabolic tissue and its contributions to T2D pathophysiology.

Here, we explored the function of IMP2 during adipogenesis and inquire whether the reduced fat mass of Imp2 null mice is due to the tissue-autonomous effect of white depots. Imp2ff mice that bear a Cre recombinase driven by platelet-derived growth factor receptor α (Pdgfrα) promoter (PIMP2-KO) exhibit a marked loss of Imp2 expression in ADSC and a notable ∼40% decrease in white adipocyte mass. However, they have normal glucose metabolism and insulin sensitivity. The reduced white adiposity is attributable to a marked reduction of preadipocyte number in PIMP2-KO mice while their preadipocytes showed normal proliferation and terminal differentiation. Mechanically, deletion of Imp2 in ADSC increases Wnt receptor Frizzled class receptor 8 (*Fzd8*) mRNAs (an Imp2 client) and polypeptides. Imp2 destabilized m^6A-modified *Fzd8* mRNA by recruiting CCR4-NOT deadenylase complex in an mTOR-dependent manner. As a summary, our studies reveal that Imp2 deletion in mesenchymal stem cell (MSC) protects mice from diet-induced obesity without affecting glucose and insulin tolerance. Imp2 is critical for the early commitment of ADSC into preadipocytes through regulating *Fzd8* mRNA stability but dispensable for preadipocyte proliferation and terminal differentiation. The interaction of Imp2 and *Fzd8* mRNA acts as a bridge between mTOR signaling and Wnt pathway to determine the lineage fate of ADSC.

RESEARCH DESIGN AND METHODS

Animal Studies

All animal procedures were approved by the Institutional Animal Care and Use Committee of Massachusetts General Hospital and were performed in accord with the National Research Council guidelines for laboratory animal care (16). Mice were maintained on the C57BL/6J background in a specific-pathogen-free facility with a 12-h light/12-h dark cycle and fed irradiated chow (Prolab 5P75 Isopro 3000, with 5% crude fat; PMI Nutrition International) or HFD (D12492i, 60% of kcal fat; Research Diets). After weaning at 4 weeks of age, sex-matched littermates were housed in the same cage with a maximum number of four mice per cage. Cages were changed every 2 weeks, and nesting material was provided. Animals were sacrificed if they had wounds from fighting, developed severe dermatitis or tumors, or showed other signs of morbidity, such as unresponsiveness to touch or not eating. Imp2 floxed mice have previously been described (17–19). PDGFRa-Cre mice were purchased from The Jackson Laboratory (stock no. 013148). All mice studies were conducted for both sexes. Data are available on request where only data for males are presented.

Body Composition, Indirect Calorimetry, Food Intake, and Activity

For analysis of body weight, body composition, and food intake, mice were kept at a normal ambient temperature of 23°C and had free access to water and food. Measurements of energy expenditure were performed with a customized indirect calorimetric system. Mice were individually housed and placed in a Promethion metabolic analyzer (Sable Systems International, Las Vegas, NV) for 3 days before recording started. Body composition was evaluated in live, conscious animals in triplicate with quantitative nuclear magnetic resonance spectroscopy (EchoMRI analyzer; Echo Medical Systems, Houston, TX).

Glucose and Insulin Tolerance Tests

For glucose tolerance tests, mice were fasted 6 h. D-glucose (20%) (1 g/kg body wt i.p.; Sigma-Aldrich, St. Louis, MO) was administered. At 0, 15, 30, 60, and 120 min after administration, blood was collected through tail vein bleeding. Glucose levels were measured with a One Touch Ultra AlphaTRAK 2 glucometer (Zoetis, Parsippany, NJ). For insulin tolerance tests, high-fat-fed mice were fasted for 6 h. Human insulin (Eli Lily) at 0.75 units/kg i.p. was injected. Blood was drawn from the tail vein after injection, and glucose levels were measured as described above.

Serum Analyses

Blood was collected into EDTA-coated tubes (Sarstedt, Newton, NC). Serum was separated by centrifugation at 4°C, frozen in liquid nitrogen, and assayed at the Vanderbilt University Mouse Metabolic Phenotyping Center.

Adipose Tissue Analysis

Subcutaneous and gonadal white adipose tissue (WAT) from age- and sex-matched PIMP2-KO and control mice was dissected. For histological analysis, tissue slices were fixed in buffered formalin and paraffin embedded. Fat cell size was determined with the Coulter counter after osmium tetroxide fixation essentially as described by Hirsch and Gallian for both sexes (20).

Adipose-Derived Stromal Vascular Cells Isolation and Proliferation Assay

Subcutaneous and gonadal WAT was dissected from PIMP2-KO and control mice, minced, and digested with use of 0.5% collagenase (Sigma-Aldrich) at 37°C for 1 h. Cell suspensions were filtered through a cell strainer with 100 μm nylon mesh (BD Biosciences, San Jose, CA) and washed twice with PBS by centrifugation for 3 min at 1,500 rpm at 4°C. Cell pellets were suspended in red

blood cell lysis buffer (Sigma-Aldrich) and incubated for 5 min. Cells were washed and centrifuged twice in PBS and incubated in DMEM (Gibco, Carlsbad, CA) with 10% FBS (Gibco) and 1% penicillin/streptomycin (Life Technologies, Carlsbad, CA) at 37°C in 5% CO_2. The media were replaced after 24 h and every 3 days thereafter. Cultures were incubated for 4–7 days until 70–80% confluence was attained. ADSC were passaged and replated at initial concentration of 5×10^5 cells per 100-mm dish. All experiments were performed with passage 2 ADSC. Cell proliferations were analyzed with WST-1 proliferation assay kit according to the manufacturer's instructions (Roche, Mannheim, Germany). In each experiment, 4×10^3 cells/well were plated in 96-well plates, and the proliferation was measured in quadruplicate at 0, 24, 48, 72, and 96 h.

Flow Cytometry of Adipose-Derived Stromal Vascular Cells

Adipose tissues were dissected from subcutaneous and gonadal fat and stromal vascular fraction was isolated. Cells labeling and sorting were performed as previously described (21). Briefly, the isolated SVF was resuspended in ice-cold DMEM with 2% FBS for labeling. Antibodies labeling was performed on ice for 20 min. Cells were washed and resuspended in sorting buffer containing 0.5g/mL propidium iodide (Sigma-Aldrich) for sorting. Cells were sorted on a BD SORP FACSAria and analyzed on a BD LSR II (BD Biosciences), each running with BD FACSDiva 6 software. For sorting, cells initially were selected by size and then by exclusion of dead cells based on propidium iodide uptake. Next, cells were separated by cell surface markers.

ADSC Differentiation

FACS-isolated ADSC cells ($CD24^+$) from pooled SVF of gonadal and subcutaneous fat were grown to confluence and induced to differentiate with use of adipogenic cocktail consisting of 10 μg/mL insulin (Sigma-Aldrich), 1 μmol/L dexamethasone (Sigma-Aldrich), and 500 μmol/L isobutylmethylxanthine (Sigma-Aldrich). After 48 h adipogenic induction, cultures were maintained in DMEM containing 10% FBS and 10 μg/mL insulin for another 7 days. Differentiated adipocytes were fixed in 4% paraformaldehyde for 45 min at room temperature. After washing with 1× PBS twice, the cells were stained with Oil Red O working solution (0.5% iso-propanol; Sigma-Aldrich) at room temperature for 30 min. The Oil Red O solution was removed, and the cells were washed with 1× PBS before imaging.

C3H10 T1/2 Cell Culture

Mouse embryonic fibroblast cells C3H10 T1/2 were purchased from ATCC (CCL-226) and cultured according to the supplier's protocol. Briefly, cells were grown in high-glucose (4.5 g/mL) DMEM supplemented with 10% FCS and 0.5% penicillin-streptomycin (v/v) at 37°C and 5% CO_2. Cells were cultured until they reached 80–90% confluence. Cells between passages 4 and 10 were used for the experiments. Flag-tagged full-length IMP2 WT, IMP2-AA, and IMP2-DD were obtained as previously described (22). IMP2-AA abolishes phosphorylation, while IMP2-DD functions as a phosphomimetic. The *Fzd8* mutant plasmids were generated with QuikChange II Site-Directed Mutagenesis Kit (Agilent Technologies). Plasmids were transfected into C3H/10T1/2 cells with Lipofectamine (Thermo Fisher Scientific) according to the manufacturer's protocol. The CRISPR/Cas9 method was used to delete Imp2 (gRNA: ACAAGAACAATTCCTGAGCT) and *Cnot1* (gRNA: GCTTGAGAACTTTACTCAGC) in C3H/10T1/2 cells as previously described (22). The lentivirus was prepared in human embryonic kidney (HEK) 293T cells, and the viral supernatant was then used to infect C3H10T1/2 cells. The cells were selected with 1 μg/mL puromycin for gene knockout and assayed with Western blots. For NSC654259 (PC-60868; ProbeChem) treatment, the compound was dissolved in DMSO to make 10 mmol/L stock solution and the final concentration of 1 μmol/L was used for experiments.

C3H10 T1/2 Adipocyte Differentiation Assay

For differentiation assay, C3H10 T1/2 cells were plated (2×10^5 cells/cm^2) in collagen I–coated 24-well plates. One day postconfluence, differentiation medium containing 10 μg/mL insulin (Sigma-Aldrich), 1 μmol/L dexamethasone (Sigma-Aldrich), 500 μmol/L isobutylmethylxanthine (Sigma-Aldrich), and 1 μmol/L rosiglitazone (Sigma-Aldrich) was added. After 48 h adipogenic induction, cultures were maintained in DMEM containing 10% FBS and 10 μg/mL insulin for another 7 days. Every 2 days, the maintenance media was replaced. Cells were lysed after 96 h for gene expression assay and after 1 week for Oil Red O staining.

Real-time PCR

Total RNA (1 mg) was used for cDNA preparation with random-hexamer primers using SuperScript III reverse transcriptase (Invitrogen). Steady-state mRNA expression was measured by quantitative real-time PCR using SYBR Green Master Mix (Bio-Rad Laboratories) with a CFX96 real-time PCR system (Bio-Rad Laboratories). All quantitative PCR primer pairs were purchased from OriGene.

Imp2 Immunoprecipitation Followed by RT-PCR

WAT from 6-week-old male mice were harvested after sacrifice and extracted directly with a TissueLyser (QIAGEN) in ice-cold lysis buffer (140 mmol/L KCl, 1.5 mmol/L $MgCl_2$, 20 mmol/L Tris-HCl at pH 7.4, 0.5% Nonidet P-40, 0.5 mmol/L dithiothreitol, 1 units/μL RNase inhibitor, one complete EDTA-free protease inhibitor cocktail tablet) and extracted for 10 min. The lysates were centrifuged for 10 min at 14,000 rpm, and the supernatant was transferred to a fresh 1.5-mL tube. Total protein was measured by a Bradford assay, and 5 mg cytoplasmic lysate protein was subjected to immunoprecipitation.

Lysates were incubated with 500 μL protein A Dynabeads magnetic beads precoated with IMP2 antibody and incubated for 6 h at 4°C with rotation. Dynabeads were extensively washed with lysis buffer five times and digested with DNase I and protease K. RNA was extracted with phenol-chloroform and precipitated with ethanol. Real-time PCR was performed to examine RNAs associated with IMP2 from subcutaneous and gonadal WAT.

Polysome Fractionation

Subcutaneous and gonadal depots were homogenized in ice-cold lysis buffer (10 mmol/L Tris [pH 7.5], 250 mmol/L KCl, 10 mmol/L $MgCl_2$, 0.5% Triton X-100, 2 mmol/L dithiothreitol, 100 g/mL cycloheximide, 100 units/mL RNase inhibitor [Thermo Fisher Scientific], and protease inhibitor cocktails [Thermo Fisher Scientific]) with a QIAGEN tissue homogenizer. Homogenates were continuously vortexed for 5 min at 4°C and incubated for 15 min on ice. Samples were then centrifuged at 10,000*g* for 10 min at 4°C. The resulting supernatant was layered on a 15%–50% linear sucrose gradient (20 mmol/L Tris [pH 7.5], 250 mmol/L KCl, 10 mmol/L $MgCl_2$) and centrifuged in an SW41 rotor at 40,000 rpm for 160 min at 4°C. After centrifugation, the gradient was displaced through a spectrophotometer, and the optical density at 254 nm was continuously recorded. Two sucrose fractions, representing the subpolysomal and polysomal portions of the gradient, were collected directly into an equal volume of TRIzol reagent (Invitrogen). RNA was extracted, and samples were analyzed for quality with the Agilent 2100 bioanalyzer (Agilent Biotechnologies). An equal quantity of RNA in each fraction was converted to cDNA.

mRNAs Half-lives Determination

Cells were treated with 1 mmol/L actinomycin D (Sigma-Aldrich) for 12 h to block transcription. After the indicated times, total RNAs were extracted, followed by DNase digestion for eliminating DNA contamination and cDNA syntheses. The concentration of mRNAs was quantified by real-time RT-PCR with the SYBR Green.

Immunoblotting

Proteins were extracted from WAT from 6- to 8-week-old HFD-fed male mice with a tissue homogenizer (QIAGEN). Subcutaneous and gonadal WAT were homogenized in ice-cold buffer (20 mmol/L Tris [pH 7.5], 2.7 mmol/L KCl, 1 mmol/L $MgCl_2$, 1% Triton X-100, 10% [wt/vol] glycerol, 1 mmol/L EDTA, 1 mmol/L dithiothreitol) supplemented with protease (Thermo Fisher Scientific) and phosphatase inhibitor cocktails (Millipore). Samples were then centrifuged at 13,000 rpm for 10 min at 4°C, and the supernatants were collected. The protein content of the supernatant was determined with a bicinchoninic acid assay (Thermo Fisher Scientific). Aliquots of each extract containing 50 μg protein were loaded for Western blotting. Proteins were resolved on a 4%–12% gradient SDS Bis-Tris gel (Invitrogen, Carlsbad, CA). Antibodies for immunoblotting are listed in Supplementary Table 1.

Nuclear and Cytoplasmic Protein Extraction

Nuclear proteins were isolated using the Nuclear Extract kit (78833; Thermo Fisher Scientific) following the manufacturer's instructions. Briefly, the cells were collected into buffer CER I and were vortexed vigorously for 15 s, followed by a 10-min incubation on ice. The ice-cold buffer CER II was added to the mixture, and the tubes were vortexed for 5 s. The samples were incubated on ice for 1 min, vortexed for another 5 s, and centrifuged for 5 min at the speed of 16,000*g* at 4°C. The supernatant containing cytoplasmic extract was immediately transferred into a new prechilled tube and further lysed in 1× Laemmli buffer. The pellet (nuclear fraction) was incubated in ice-cold NER buffer for a total of 40 min and vortexed for 15 s every 10 min. The lysate was centrifuged at maximum speed for 10 min at 4°C for collection of the supernatant (nuclear extract).

Protein Half-life Determination

Cycloheximide was used at a final concentration of 250 mmol/L to inhibit mRNA translation; protein half-life was determined with immunoblots of extracts prepared before and at various times after cycloheximide addition.

Statistical Analysis

Comparisons between the mean ± SD of two groups were calculated with two-way ANOVA or Student unpaired two-tailed *t* test. *P* values of ≤ 0.05 were considered statistically significant.

Data and Resource Availability

All data and resources are available on request.

RESULTS

Imp2 Deletion in Mouse MSC Protects Against Diet-Induced Obesity

To define IMP2's function in adipogenesis, we first examined Imp2 expression in WAT. The level of Imp2 polypeptide is mostly enriched in ADSC followed by preadipocytes from SVF; mature adipocytes have the lowest level of Imp2 protein (Fig. 1*A*). We next crossed Pdgfrα-Cre mice with $Imp2^{lox+/+}$ mice to delete Imp2 in ADSC. PDGFRα is a membrane-bound tyrosine kinase receptor expressed in perivascular stromal cells within a variety of tissues (23) and have commonly been used as a cell surface marker for MSC identification (24). As expected, the Imp2 expression in ADSC was greatly reduced in PDGFRα-$Cre^{+/-}$/$Imp2^{lox+/+}$ (PIMP2-KO) mice but was similar in mature adipocytes compare with controls (Fig. 1*B*). The fat mass of PIMP2-KO mice fed on HFD is consistently lower after weaning (Fig. 1*C*), whereas lean body mass was not different from control animals for both sexes

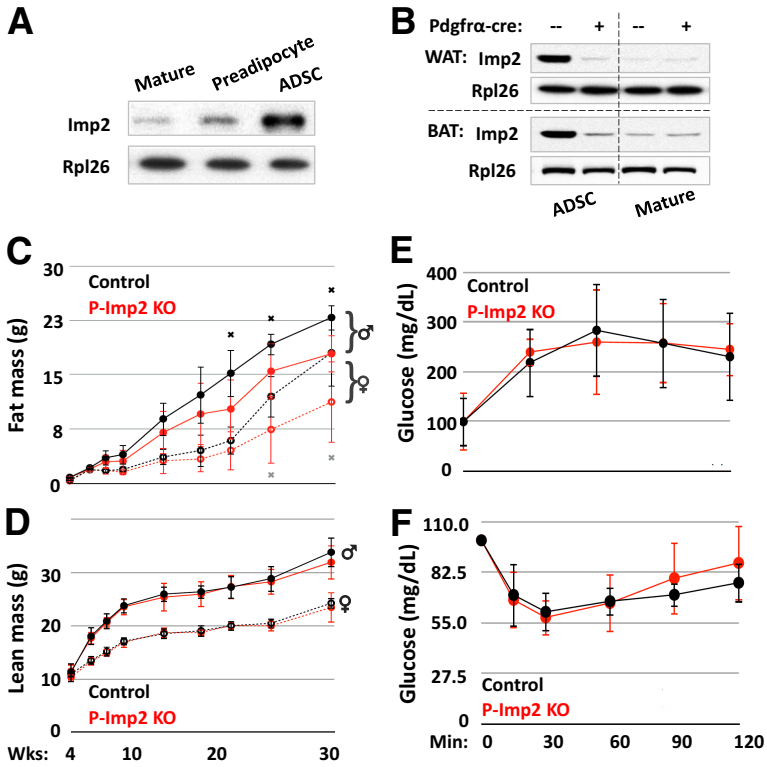

Figure 1—Imp2 deletion in ADSC leads to resistance to diet-induced obesity but has no effect on glucose tolerance or insulin sensitivity. *A*: Imp2 immunoblotting of ADSC and mature adipocytes from 4-week-old, male mice fed on NCD. *B*: Representative images of male mice fed on HFD for 30 weeks and their gonadal fat depot. *C* and *D*: The accumulation of fat (*C*) and lean (*D*) mass of mice on HFD. Control male, $n = 8$; PIMP2-KO male, $n = 6$; control female, $n = 10$; PIMP2-KO female, $n = 9$. *E*: Glucose tolerance test of 14-week-old, HFD-fed male mice ($n = 8$ pairs). *F*: Insulin tolerance test of 16-week-old, HFD-fed male mice ($n = 8$ pairs). Data are means ± SE. *t* test, $^*P < 0.05$. BAT, brown adipose tissue; Wks, weeks.

(Fig. 1*D*). The total body weight of male and female PIMP2-KO mice fed HFD is consistently lower than that of controls, with statistical significance reached at ∼30 weeks (Supplementary Fig. 1*A*). The PIMP2-KO mice displayed normal body size, food intake, energy expenditure, and physical activity (Supplementary Fig. 1*B*–*E*). Consistent with reduced white fat mass, serum leptin level is lower in PIMP2-KO mice (Table 1). However, fasting blood glucose and serum insulin levels were similar between PIMP2-KO and control mice (Table 1). Glucose tolerance and insulin sensitivity were also not different on either HFD or NCD (Fig. 1*E* and *F* and Supplementary Fig. 1*E* and *F* and Supplementary Fig. 2). Based on the above data, we conclude that PDGFRα-Cre$^{+/-}$/Imp2$^{lox+/+}$ mice are resistant to diet-induced obesity, although to an extent that does not alter glucose metabolism and insulin sensitivity.

IMP2 Determines Mature White Adipocyte Cell Number

Next, we tried to determine the cellular basis for the decreased WAT mass in PIMP2-KO (Fig. 2*A*) and analyzed hematoxylin-eosin (H-E)-stained histological sections of white fat pads. The results of H-E showed that PIMP2-KO mice have similar mature adipocyte size similar to that of controls (Fig. 2*B*), suggesting that the decreased white adipocyte mass in PIMP2-KO is due to decreased mature adipocyte cell number. This was confirmed by studies of the osmium tetroxide–fixed adipocytes. While the radius of mature adipocytes is not different (Fig. 2*C*) between PIMP2-KO and control, the number of mature adipocytes from PIMP2-KO was reduced ∼40% for both gonadal and subcutaneous depots of HFD-fed mice (Fig. 2*D*). Similar phenotypes have also been observed for male PIMP2-KO

Table 1—Average blood glucose, insulin, leptin, and liver triglyceride level of 28-week-old HFD-fed male and NCD-fed female mice

	Fast glucose (mg/dL)	Insulin (pg/mL)	Leptin (pg/mL)	Liver TG (mg/dL)
HFD male				
Control ($n = 8$)	221	5,024	7,326	87
PIMP2-KO ($n = 8$)	218	4,860	3,945	69
P value (*t* test)	0.32	0.53	0.03	0.14
NCD female				
Control ($n = 7$)	124	3,684	841	119
PIMP2-KO ($n = 6$)	125	3,323	639	115
P value (*t* test)	0.84	0.72	0.02	0.76

TG, triglyceride.

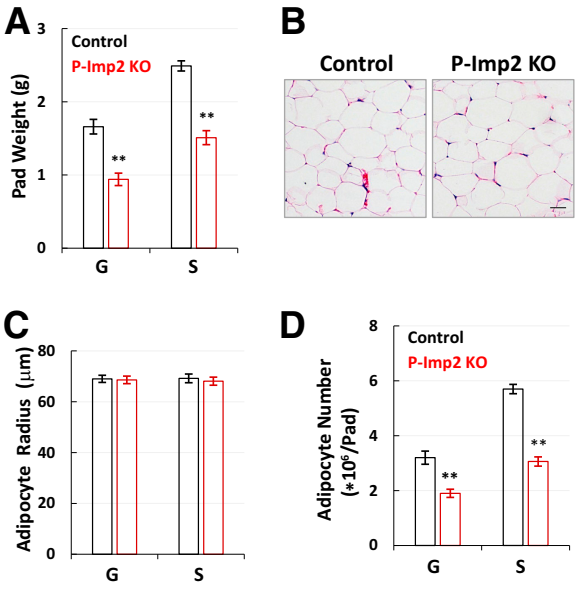

Figure 2—Imp2 deletion in ADSC reduces mature adipocyte number. *A*: The relative white adipocyte tissue weight of 28-week, HFD-fed male mice. G, gonadal fat; S, subcutaneous fat. *B*: Representative H-E images of gonadal fat from HFD-fed male mice at 28 weeks. Scale bar: 50 μm. *C* and *D*: Mature adipocytes size (*C*) and number (*D*) of 28-week-old HFD-fed male mice (n = 6 pairs). Data are means ± SD. t test, $^{**}P < 0.01$.

mice fed on NCD (Supplementary Fig. 2*D–F*). Therefore, the WAT depots of PIMP2-KO mice contain reduced number of mature adipocytes of a size similar to that of control white adipocytes.

Imp2 Promotes the Commitment of MSC to Adipogenic Lineage

We next sought to determine the role of Imp2 in the adipogenic development and first isolated preadipocytes (Lin^+/$CD29^+$/$CD34^+$/$Sca1^+$/$CD24^-$ cells) from SVF of pooled samples of gonadal and subcutaneous adipose tissues. Surprisingly, this cell population was reduced by ∼50% in PIMP2-KO mice (Fig. 3*A*), suggesting that Imp2 is critical for the early commitment of MSC into the adipogenic lineage. Consistent with flow cytometry data, the mRNA expression of *Pdgfβ*, *Dlk1*, and *Vcam1* greatly decreased in ADSC ($CD24^+$ cells) isolated from P-IMP2 KO mice (Fig. 3*B–D*). Furthermore, *Cebpα* and *Pparγ* mRNA from differentiated PIMP2-KO ADSC also decreased (Fig. 3*E* and *F*), indicating that the adipogenic potential of PIMP2-KO is impaired. Next, we examined the role of Imp2 in terminal differentiation. When seeded at the same density, preadipocytes from WAT depots of PIMP2-KO mice showed normal proliferation (Supplementary Fig. 3*A*) and normal terminal differentiation (Supplementary Fig. 3*B*). In summary, Imp2 deletion in ADSC reduces the number of preadipocytes but does not impair their ability to proliferate or differentiate into mature adipocytes.

Imp2 Binds *Fzd8* mRNA and Promotes Its Degradation

We previously performed proteomics and RNA-sequencing analysis of Imp2 null mouse embryonic fibroblast cells (22) and observed significantly upregulated Wnt/β-catenin signaling, which is known to inhibit the commitment of MSC to adipocytes (3). Therefore, we examined the mRNA and protein expressions of key factors (25) of canonical Wnt pathway in PIMP2-KO ADSC (Fig. 4*A* and *B*). Consistent with mouse embryonic fibroblast data, the expression of Frizzled (Fzd) polypeptides (Fzd8/Fzd2) and the receptor of Wnt signaling pathway (Wnt10a) was increased in PIMP2-KO ADSC, especially for Fzd8 (Fig. 4*C*). For identification of Imp2 mRNA clients during adipogenesis, immunoprecipitates (IPs) were prepared from extracts of ADSC isolated from 4-week-old mice using anti-Imp2 antibody. Compared with IPs obtained with nonimmune IgG, the Imp2 IP was substantially enriched in mRNAs encoding *Fzd8*, whereas the enrichment of other mRNAs examined was not significantly different (Fig. 4*D*). In line with increased Fzd8 protein abundance, the elevated β-catenin polypeptides from nucleus were observed in PIMP2-KO ADSC (Fig. 4*E*). Moreover, the transcripts of β-catenin directly regulated genes, such as *Ccnd1*, *C-Myc*, *Mmp7*, and *Itf2*, are consistently increased in PIMP2-KO ADSC (25) (Fig. 4*F*).

Imp2 Binds *Fzd8* mRNA in an m^6A-Dependent Manner

To understand the mechanisms by which Imp2 regulates *Fzd8* mRNA abundance, we inactivated Imp2 by CRISPR in the MSC-like cell line C3H10T1/2 and examined the binding of Imp2 with *Fzd8* mRNA (Fig. 5*A*). Compared with CRISPR GFP control C3H10T1/2 cells, Imp2 CRISPR cells exhibit ∼10-fold increase of the abundance of *Fzd8* mRNA and protein (Fig. 5*B* and *C*), accompanied by a significantly prolonged mRNA half-life (Fig. 5*D*), but unaltered protein half-life (Fig. 5*E*). The polysomal abundance of *Fzd8* mRNA was not altered by Imp2 deletion (Fig. 5*F*), suggesting a normal translation of *Fzd8* mRNA. Thus, the increased Fzd8 polypeptide abundance in the IMP2 null C3H10T1/2 cells is due to increased *Fzd8* mRNA stability and Imp2 is required to promote *Fzd8* mRNA degradation.

The m^6A modification is known to regulate the stability of the modified RNAs through the recruitment of specific "reader" proteins (26,27). IMPs have been shown to selectively recognize and bind to m^6A consensus sequence RR(m^6A)CH (R = A, G, or U; R = A or G; and H = A, C, or U) which is near stop codons and enriched in the 3′-untranslated regions (28,29). Therefore, we hypothesized that Imp2 controls *Fzd8* mRNA stability through m^6A recognition. Using *Fzd8*-specific m^6A assays, we find that *Fzd8* mRNAs preferably bind with m^6A antibodies (Fig. 5*G*), indicating m^6A modification of *Fzd8* mRNAs. Notably, the *Fzd8* mRNA stop codon containing region has mostly predicted m^6A modifications that overlap with conserved IMP2 binding sites (Fig. 5*H* and *I*). To test whether this region is critical for Imp2-regulated *Fzd8* mRNA stability, we inserted the 160 nt wild-type or mutant

A

Genotype	Control	P-Imp2 KO	p-value
BW (g)	21.5	20.3	0.12
PG (g)	0.3	0.3	0.35
SC (g)	0.3	0.2	0.64
Lin1$^-$ (%)	100	100	1
CD29$^+$(%)	18.4	15.2	0.49
CD34$^+$(%)	**9.6**	**5.1**	**0.01**
Sca1$^+$ (%)	**8.1**	**4.2**	**0.01**
CD24$^+$ (%)	0.9	0.7	0.55
CD24$^-$ (%)	**5.8**	**2.8**	**0.02**

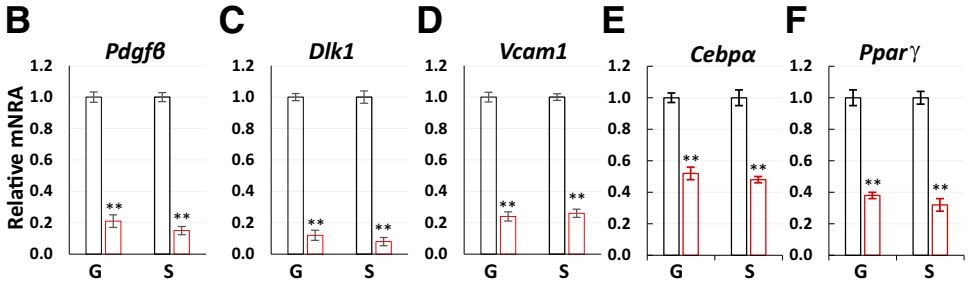

Figure 3—Imp2 is essential for the commitment of MSC to ADSC. *A*: Enumeration of ADSC in control and PIMP2-KO WAT. The gonadal (G) and subcutaneous (S) WAT depots from 28-week-old male mice fed on HFD were digested with collagenase; the stromal vascular cells were labeled with antibodies to the surface markers indicated and separated by flow cytometry, and the CD24$^+$ and CD24$^-$ adipocyte precursors from each mouse were enumerated individually. The average and *P* value are shown. *B–F*: The gonadal and subcutaneous WAT depots excised from 4-week-old male mice were digested. Control, black; PIMP2-KO, red. *B–D*: The relative mRNA expression of *Pdgfβ*, *Dlk1*, and *Vcam1* in ADSC. *E* and *F*: The relative *Cebpα* and *Pparγ* mRNA in differentiated ADSC. The mRNA was extracted from cells at 4th day of differentiation. Data are means ± SD. *t* test, $^{**}P < 0.01$.

sequence flanking stop codon of *Fzd8* mRNA into *Fzd8* coding region (Supplementary Fig. 4) and transfected them into C3H10T1/2 cells. IMP2 RNA immunoprecipitation–quantitative PCR showed a strong binding of IMP2 with wild-type *Fzd8* mRNA but not with the mutant form (Fig. 5*J*). Moreover, the half-life of *Fzd8* m6A mutant increased approximately sixfold via the *Fzd8* wild-type mRNA (Fig. 5*K*). Taken together, our data demonstrate that Imp2 selectively binds m^{6}A-methylated *Fzd8* mRNA and controls its decay.

Imp2 Interacts With CCR4-NOT Deadenylase Complex

Intracellular RNA degradation occurs by two major pathways starting from the 5′ end or the 3′ end of the RNA, respectively. IMP1 has been reported to interact with CNOT1 directly (30), which is the scaffold protein of the CCR4-NOT complex, an important deadenylase responsible for poly(A) tail shortening and inducing 3′-5′ decay of numerous RNAs in the cytoplasm. We therefore hypothesized that IMP2 associates with components of the RNA decay machinery to control *Fzd8* mRNA degradation. To test this hypothesis, we performed Imp2 IP in C3H10T1/2 cells and confirmed the interaction of IMP2 with CNOT1 (Fig. 6*A*). If the interaction between IMP2 and CNOT1 is crucial for the *Fzd8* mRNA stability, the depletion of CNOT1 will increase the expression level of *Fzd8* transcript. As expected, a marked increase in the abundance of *Fzd8* mRNA was observed after Cnot1 expression was abolished (Fig. 6*B* and *C*). Moreover, the depletion of Imp2 and Cnot1 simultaneously had no additive effect on *Fzd8* mRNA upregulation (Fig. 6*B* and *C*), indicating that the two proteins are mechanistically linked in determining the abundance of *Fzd8* mRNA. Therefore, by associating with CNOT1, IMP2 recruits the CCR4-NOT deadenylase complex onto *Fzd8* mRNA and promotes its degradation.

Imp2 Destabilization of *Fzd8* mRNA Requires Acidic Charges at the mTOR Phosphorylation Sites

We previously published that mTOR directly phosphorylates IMP2 at Ser162Ser164. To evaluate the functional significance of Ser162Ser164 for the ability of IMP2 to

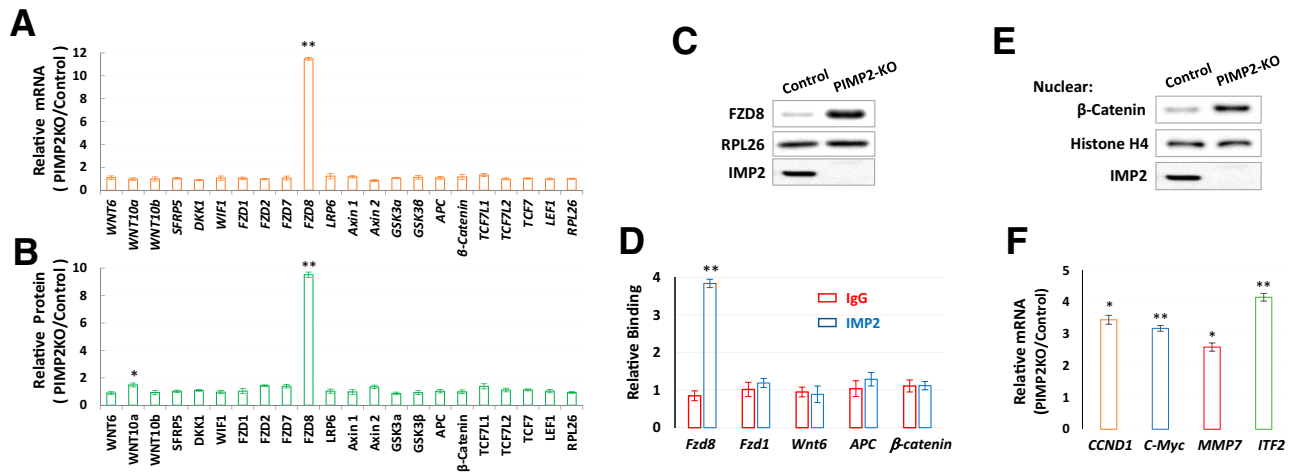

Figure 4—IMP2-deficient ADSC showed elevated FZD8 expression. *A*: Relative protein abundance of PIMP2-KO/control from stromal vascular cells of 4-week-old, HFD-fed male mice (n = 9 pairs). *B*: The immunoblotting of FZD8 in stromal vascular cells from 4-week-old, HFD-fed male mice (n = 3 pairs). *C*: Relative binding of mRNAs in immunoprecipitation of IgG (red) and IMP2 (blue). *D*: Western blots of β-catenin in nuclear extract of stromal vascular cells from 4-week-old, HFD-fed male mice (n = 4 pairs). *E*: Relative mRNA expression of β-catenin transcriptionally regulated genes. RNA was isolated from 6-week-old, HFD-fed male mice (n = 5 pairs). Data are means ± SD. t test, $^*P < 0.05$, $^{**}P < 0.01$.

control *Fzd8* mRNA stability, we generated IMP2 variants with Ala or Asp at both Ser162 and Ser164, which we refer to as IMP2-AA (nonphosphorylatable) and IMP2-DD (phosphomimetic), and stably expressed them in IMP2-deficient C3H10T1/2 cells. Polyclonal populations were selected. The half-life of *Fzd8* mRNA from C3H10T1/2 cells expressing IMP2-DD was substantially shorter than wild type IMP2 (Fig. 6*D*); whereas the half-life of *Fzd8*

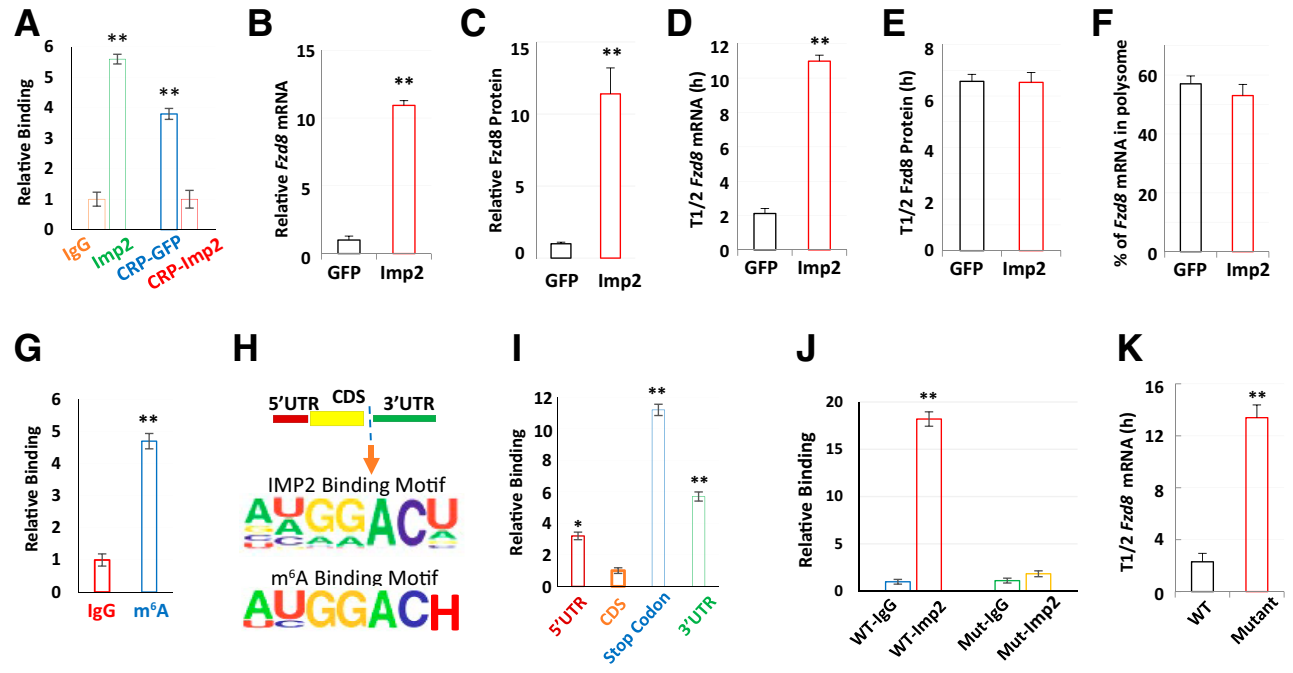

Figure 5—Imp2 directly binds *Fzd8* mRNA and promotes its degradation in an m^{6}A-dependent manner. *A*: Imp2 binds *Fzd8* mRNA. IPs were performed with nonimmune IgG and anti-Imp2 antibody (left pair) or from the Imp2-IP using cell extracts of CRP-GFP and CRP-Imp2 (right pair). *B*: Relative *Fzd8* mRNA in CRISPR GFP or IMP2 C3H10 cells. *C*: Relative *Fzd8* protein in CRISPR GFP or Imp2 C3H10 cells. *D*: The half-life of *Fzd8* mRNA in CRISPR GFP or IMP2 C3H10 cells. *E*: The half-life of Fzd8 protein in CRISPR GFP or Imp2 C3H10 cells. *F*: The percentage of *Fzd8* mRNA in polysome from CRISPR GFP or Imp2 C3H10 cells. *G*: The enrichment of *Fzd8* mRNA with nonimmune IgG and m^{6}A antibody. *H*: The Imp2 and m^{6}A binding motif around the stop codon of *Fzd8* gene. CDS, coding sequence. *I*: The enrichment of Imp2 binding sites on different locations of *Fzd8* mRNA. *J*: The relative binding of wild-type (WT)/m^{6}A mutant (Mut) *Fzd8* mRNA with Imp2 and IgG control. *K*: The half-life of wild-type and m^{6}A mutant *Fzd8* mRNA. Data are means ± SD. t test, $^{**}P < 0.01$.

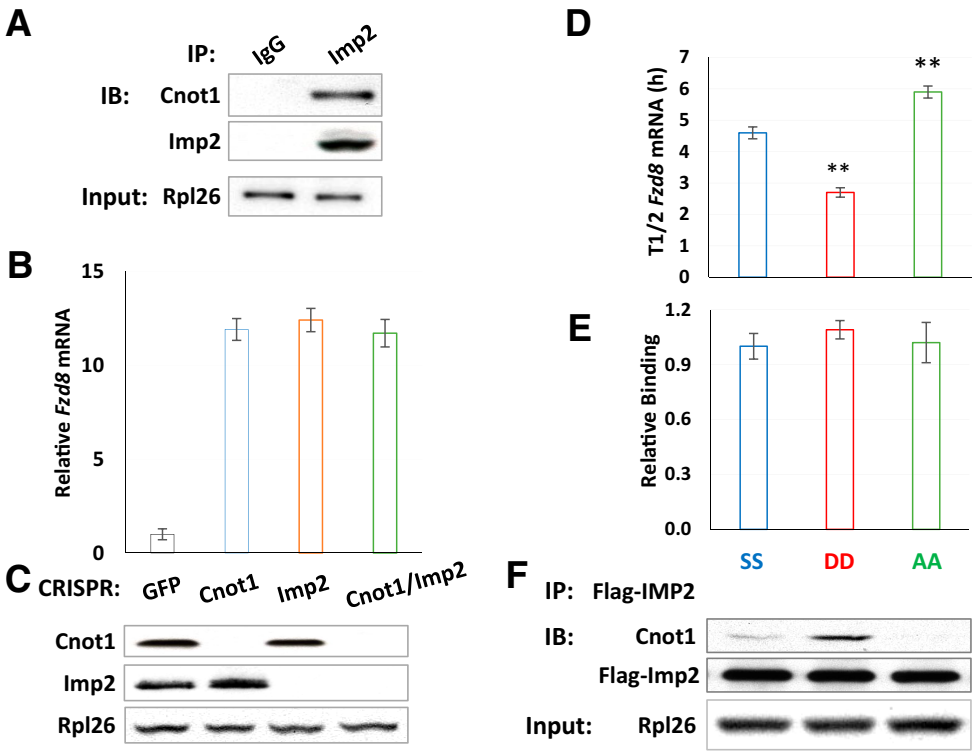

Figure 6—The destabilization of *Fzd8* mRNA by Imp2 is mediated by Cnot1 and requires acidic charges of Imp2 at the mTOR phosphorylation sites. *A*: Imp2 interacts with Cnot1 in C3H10 cells. Imp2 and IgG immunoprecipitations were performed using extraction of rapidly growing C3h10 cells and blotted for Cnot1. *B* and *C*: The relative *Fzd8* mRNA abundance (*B*) and polypeptide expression of Cnot1 and IMP2 (*C*) in CRISPR *Cnot1, Imp2, Cnot1/Imp2*, and GFP C3H10 cells. *D*: The half-life of *Fzd8* mRNA in stable C3H10 cells of Imp2 phosphorylation variants. *E*: Relative binding of *Fzd8* mRNA with IMP2 phosphorylation variants. *F*: The Western blot of Cnot1 from Flag-IMP2 immunoprecipitation. Flag immunoprecipitations were performed using extraction of rapidly growing, stable IMP2-SS, DD, and AA C3H10 cell lines. Data are means ± SD. *t* test, $^{**}P < 0.01$. IB, immunoblotting.

mRNA from IMP2-AA stable cells showed significantly prolonged half-life compare to wild type IMP2 (Fig. 6*D*). As IMP2 controls RNA life cycle through binding affinity (4), we examined IMP2 variants' ability to bind *Fzd8* mRNA. Unexpectedly, all IMP2 P-site mutants bind *Fzd8* mRNA equally as well as IMP2 wild type (Fig. 6*E*), indicating that the IMP2 phosphorylation-dependent *Fzd8* mRNA degradation is not achieved through affecting the protein-mRNA interaction. Next, we examined the association of IMP2 variants with Cnot1. The Western blot showed that IMP2-DD has stronger interaction with Cnot1 relative to wild-type IMP2 and IMP2-AA (Fig. 6*F*). Therefore, the acidic charges at IMP2 Ser162Ser164 promote degradation of *Fzd8* mRNA through regulating the recruitment of deadenylase complex CCR4-NOT to Imp2-*Fzd8* mRNA ribonucleoprotein (RNP).

Finally, we treated Imp2 null ADSC with NSC654259, a small molecule that specifically binds to the Wnt binding site on the FZD8 cysteine-rich domain. The treatment led to reduced phosphorylation of Lrp6, a Wnt coreceptor (Fig. 7*A*), decreased β-catenin abundance (Fig. 7*B*), elevated expression of preadipocyte markers (Fig. 7*C*), and significant induction of adipogenesis (Fig. 7*D* and Supplementary Fig. 5*A* and *B*). This experiment demonstrated that inhibition of FZD8 function can rescue the reduced adipogenesis of Imp2-deficient ADSC. Together, our data showed that Imp2 is required for the commitment of MSC to adipocyte lineage by regulating *Fzd8* mRNA degradation (Fig. 7*E*).

DISCUSSION

Contribution of IMP2 to T2D Susceptibility

Worldwide obesity has nearly tripled since 1975. A consequence of this is the increased susceptibility of many pathologies such as T2D. Excessive adiposity is a major cause of obesity and insulin resistance, a main risk of T2D. Therefore, it is critical to understand the root mechanisms responsible for the development and maintenance of normal WAT.

In 2007, genome-wide association studies identified the association of SNPs within the human *IMP2* gene with increased risk for T2D. This was unexpected, as no role for IMP2 in nutrient metabolism had previously been reported. Subsequently, we found that mice with global deficiency of Imp2 exhibit a complex metabolic phenotype dominated by a reduced white fat mass with a marked resistance to diet-induced obesity and fatty liver (15). Seeking to understand the contribution of IMP2 to T2D susceptibility and its function in major metabolic tissues, we further generated and characterized mice

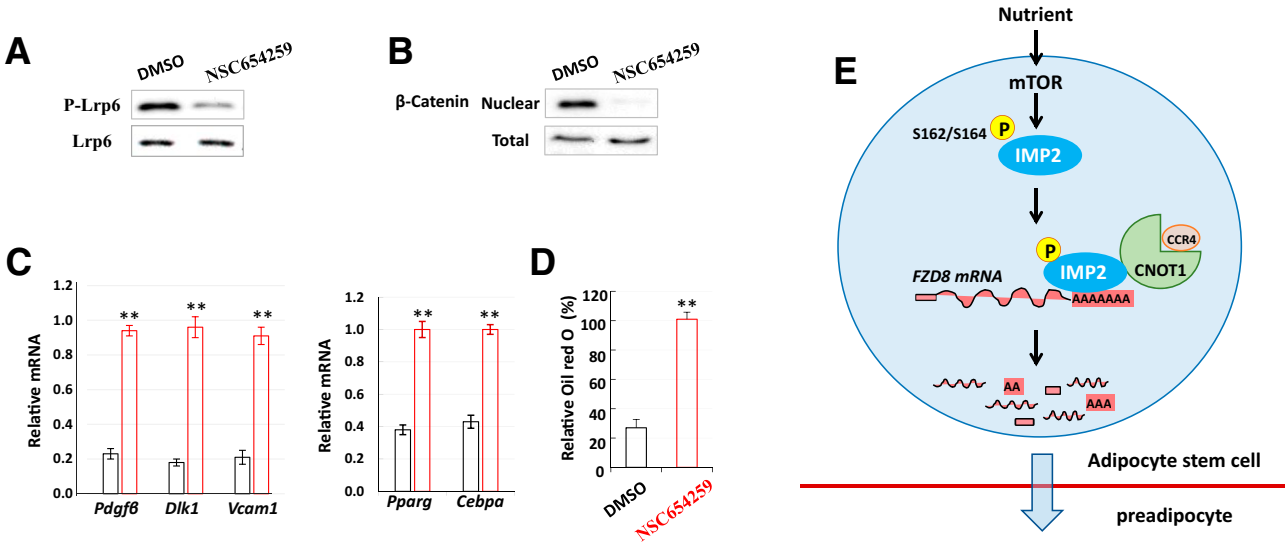

Figure 7—Inhibition of Fzd8 rescues the impaired adipogenesis of Imp2 null ADSC. *A*: The immunoblotting of total and phosphorylated (S1490) Lrp6 in DMSO- and NSC654259-treated Imp2 null ADSC. *B*: The immunoblotting of total and nuclear β-catenin in DMSO- and NSC654259-treated Imp2 null ADSC. *C*: The relative mRNA abundance of *Pdgfβ*, *Dlk1*, *Vcam1*, *Cebpα*, and *Pparγ* from Imp2 null ADSC treated with DMSO (black) and NSC654259 (red). *Cebpα* and *Pparγ* mRNAs were measured at 4th day of differentiation. *D*: The triglyceride content of DMSO- and NSC654259-treated Imp2 null ADSC at final differentiation. *E*: Schematic of mTOR-IMP2 activation of CNOT1/CCR4 complex–mediated *FZD8* mRNA degradation during the commitment of MSC to adipocyte stem cells. Data are means ± SD. *t* test, $^{**}P < 0.01$.

with tissue-specific Imp2 deficiency. Mice with pancreatic β-cell–specific Imp2 deletion showed hyperglycemia due to impaired β-cell proliferation and insulin secretion on HFD feeding (17). This discovery is consistent with findings that people with causal variants in *IMP2* gene have reduced IMP2 expression and decreased insulin secretion in islets (13,14). Studies of muscle-specific Imp2 null mice revealed that Imp2 promotes protein synthesis in skeletal muscle mass and optimizes muscle metabolism during voluntary exercise (18). Mice with hepatocyte-specific IMP2 deficiency showed diet-induced fatty liver due to reduced fatty acid oxidation (19). Reported here, the ADSC-specific loss of Imp2 impairs white fat accumulation and protects mice from diet-induced obesity. However, mice bearing Imp2 deletion in muscle, liver, and adipocyte tissues all have normal glucose tolerance and insulin sensitivity until 30 weeks old. Therefore, the collected data to date demonstrate that Imp2 contributes to T2D susceptibility primarily through β-cell insulin secretion; any strong evidence for *IMP2* association with insulin sensitivity is lacking.

Imp2 Is Required to Determine the Early Commitment of MSC to Adipogenic Lineage

The timing, dosage, and location of gene expression are fundamental determinants of different cell types such as MSC and ADSC. IMPs regulate RNA life cycle in a transcriptome-specific manner (4). The abundance of IMP1–3 polypeptides and of their client RNAs both contribute to the regulation.

White adipocytes are derived from MSC. When MSC undergo adipogenesis, they first differentiate into preadipocytes, a proliferative adipocyte precursor cell, after which they undergo terminal differentiation into mature adipocytes. During this biological process, the abundancy of IMP2 polypeptides is most enriched in isolated mouse MSC (>10×) compared with preadipocytes and mature adipocytes (Fig. 1*A*). Little or no *Imp2* expression was observed days 4–5, and virtually no *Imp2* expression remains in fully differentiated cells day 7 (Ning Dai, unpublished data). This is consistent with the general expression pattern of IMPs: highly abundant in stemness/undifferentiated state and very low in mature/differentiated state (31,32). As IMPs are considered "onco-fetal" gene to stimulate cell growth and proliferation, it is not surprising to see that Imp2 null preadipocytes proliferated and differentiated normally in vitro. This result could be due to the relative low expression of Imp2 in preadipocytes, a more differentiated cell type compared with MSC, in which Imp2 is not critical enough for their growth and differentiation. Alternatively, it could be that in vitro experimental conditions may not accurately mimic the microenvironmental milieu or stem cell niche necessary to support proliferation and differentiation. Another limitation of the study is that we could not rule out the contribution of extra-adipose to the phenotype of the PIMP2-KO mice, since PDGFRα is expressed in perivascular stromal cells within a variety of tissues. Future in vivo lineage tracing experiments will help to justify the observation based on in vitro differentiation assays.

Cross Talk of mTOR and Wnt Signaling During the Early Commitment of MSC to ADSC

mTOR pathway is the major nutrient-sensitive regulator of growth and is the key link between the availability of nutrients in the environment and the control of anabolic and catabolic processes in the body (33). mTOR is a serine/threonine protein kinase. In mammals, it constitutes the catalytic subunit of two distinct complexes known as mTOR complex 1 (mTORC1) and mTORC2 (33). These complexes are distinguished by their accessory proteins and their differential sensitivity to rapamycin, as well as by their unique substrates and functions. mTORC1 is the major nutrient sensor complex (34–36). The components of mTORC1 such as Raptor, S6K, and 4E-BPs are essential for the development of adipocyte tissues (37–39). As WAT is the largest repository of energy, previous mTOR studies mostly focus on its function in adipocyte differentiation: increasing the synthesis and deposition of triglycerides (40).

Wnt/β-catenin signaling is well-known to regulate MSC fate by inhibiting adipogenesis and promoting osteoblastogenesis (41). The signaling initiates on binding of Wnt ligands to the seven-pass transmembrane receptor FZDs and the single-pass low-density lipoprotein receptor–related protein 5 or 6 (LRP5/6) on the cell surface. This event further triggers phosphorylation of LRP5/6 and inactivation of β-catenin destruction complex. As the core receptor of Wnt proteins, the strength of the Wnt/β-catenin signaling pathway is exquisitely sensitive to the level of FZDs on the plasma membrane (42). Regulation of FZDs has emerged as a key regulatory node of the Wnt signaling pathway (43,44).

Disturbed mTOR or Wnt signaling has been implicated in numerous diseases. Both signalings play important roles in adipose tissue development: the former by acting to induce adipogenesis and the latter acting to inhibit it. Cross talk between the mTOR and Wnt signaling pathways has been reported to occur at different levels and in different cellular contexts (45–47). Whether these two fundamental pathways couple to exert physiological functions during adipogenesis remains mysterious. The data presented here demonstrate that mTOR and Wnt signaling pathways exhibit crosstalk at the level of FZDs during the early commitment of MSCs into ADSCs into preadipocytes: mTOR induces phosphorylation of IMP2, promotes the binding of IMP2 with CCR4-NOT deadenylase complex, stimulates the *Fzd8* mRNA degradation and destruct β-catenin. Thus, the IMP2/*FZD8* mRNA interaction acts as a mechanistic bridge between the mTOR and Wnt pathways to regulate the commitment of MSC into adipocytes, which could play a role in the pathophysiology of metabolic diseases.

In summary, our study demonstrated that mice with Imp2 MSC-specific deletion have reduced WAT and are resistant to diet-induced obesity, although to an extent that does not alter glucose metabolism and insulin sensitivity. Imp2 plays a key role in WAT development by stimulating the early commitment of MSC into adipogenic lineage, but it is dispensable for preadipocytes proliferation and terminal differentiation. At the molecular level, Imp2 destabilized *Fzd8* mRNA by recruiting CCR4-NOT complex in an mTOR-dependent way during MSC commitment. The data highlight the importance of posttranscriptional regulation of gene expression in maintaining WAT homeostasis. This study expands our knowledge of the cross talk between mTOR and Wnt signaling during adipogenesis and may help with discovery of new treatment and prevention of obesity, and the subsequent metabolic dysregulation.

Acknowledgments. The authors thank the MGH microscopy core of the program in membrane biology for imaging and Dr. Peroni at Brighgam and Woman's Hospital for adipocyte size determination.

Funding. This work was supported by National Institutes of Health grants DK17776 and DK057521 and Massachusetts General Hospital (MGH) institutional funds.

Duality of Interest. No potential conflicts of interest relevant to this article were reported.

Author Contributions. J.A., H.W., and N.D. conceptualized the studies; L.R., W.W., F.J., H.W., F.J., and N.D. conducted research; J.A. and N.D. wrote the original draft; W.W., H.W., J.A., and N.D. reviewed and edited the manuscript; H.W. and N.D. supervised the studies; and H.W. and N.D. administrated the whole project. N.D. is the guarantor of this work and, as such, had full access to all the data in the study and takes responsibility for the integrity of the data and the accuracy of the data analysis.

References

1. Ghaben AL, Scherer PE. Adipogenesis and metabolic health. Nat Rev Mol Cell Biol 2019;20:242–258

2. Liu GY, Sabatini DM. mTOR at the nexus of nutrition, growth, ageing and disease. Nat Rev Mol Cell Biol 2020;21:183–203

3. de Winter TJJ, Nusse R. Running against the Wnt: how Wnt/β-catenin suppresses adipogenesis. Front Cell Dev Biol 2021;9:627429

4. Dai N. The diverse functions of IMP2/IGF2BP2 in metabolism. Trends Endocrinol Metab 2020;31:670–679

5. Huang H, Weng H, Sun W, et al. Recognition of RNA N^6-methyladenosine by IGF2BP proteins enhances mRNA stability and translation. Nat Cell Biol 2018;20:285–295

6. Nielsen J, Christiansen J, Lykke-Andersen J, Johnsen AH, Wewer UM, Nielsen FC. A family of insulin-like growth factor II mRNA-binding proteins represses translation in late development. Mol Cell Biol 1999;19:1262–1270

7. Bell JL, Wächter K, Mühleck B, et al. Insulin-like growth factor 2 mRNA-binding proteins (IGF2BPs): post-transcriptional drivers of cancer progression? Cell Mol Life Sci 2013;70:2657–2675

8. Dai N, Rapley J, Angel M, Yanik MF, Blower MD, Avruch J. mTOR phosphorylates IMP2 to promote IGF2 mRNA translation by internal ribosomal entry. Genes Dev 2011;25:1159–1172

9. Dai N, Christiansen J, Nielsen FC, Avruch J. mTOR complex 2 phosphorylates IMP1 cotranslationally to promote IGF2 production and the proliferation of mouse embryonic fibroblasts. Genes Dev 2013;27:301–312

10. Saxena R, Voight BF, Lyssenko V, et al.; Diabetes Genetics Initiative of Broad Institute of Harvard and MIT, Lund University, and Novartis Institutes of BioMedical Research. Genome-wide association analysis identifies loci for type 2 diabetes and triglyceride levels. Science 2007;316:1331–1336

11. Scott LJ, Mohlke KL, Bonnycastle LL, et al. A genome-wide association study of type 2 diabetes in Finns detects multiple susceptibility variants. Science 2007;316:1341–1345

12. Zeggini E, Weedon MN, Lindgren CM, et al.; Wellcome Trust Case Control Consortium (WTCCC). Replication of genome-wide association signals in UK samples reveals risk loci for type 2 diabetes. Science 2007;316:1336–1341
13. Greenwald WW, Chiou J, Yan J, et al. Pancreatic islet chromatin accessibility and conformation reveals distal enhancer networks of type 2 diabetes risk. Nat Commun 2019;10:2078
14. Bysani M, Agren R, Davegårdh C, et al. ATAC-seq reveals alterations in open chromatin in pancreatic islets from subjects with type 2 diabetes. Sci Rep 2019;9:7785
15. Dai N, Zhao L, Wrighting D, et al. IGF2BP2/IMP2-deficient mice resist obesity through enhanced translation of Ucp1 mRNA and other mRNAs encoding mitochondrial proteins. Cell Metab 2015;21:609–621
16. National Research Council. *Guide for the Care and Use of Laboratory Animals*. 8th ed. Washington, DC, National Academies Press, 2011
17. Regué L, Zhao L, Ji F, Wang H, Avruch J, Dai N. RNA m6A reader IMP2/IGF2BP2 promotes pancreatic β-cell proliferation and insulin secretion by enhancing PDX1 expression. Mol Metab 2021;48:101209
18. Regué L, Ji F, Flicker D, et al. IMP2 increases mouse skeletal muscle mass and voluntary activity by enhancing autocrine insulin-like growth factor 2 production and optimizing muscle metabolism. Mol Cell Biol 2019;39:e00528-18
19. Regué L, Minichiello L, Avruch J, Dai N. Liver-specific deletion of IGF2 mRNA binding protein-2/IMP2 reduces hepatic fatty acid oxidation and increases hepatic triglyceride accumulation. J Biol Chem 2019;294:11944–11951
20. Hirsch J, Gallian E. Methods for the determination of adipose cell size in man and animals. J Lipid Res 1968;9:110–119
21. Rodeheffer MS, Birsoy K, Friedman JM. Identification of white adipocyte progenitor cells in vivo. Cell 2008;135:240–249
22. Dai N, Ji F, Wright J, Minichiello L, Sadreyev R, Avruch J. IGF2 mRNA binding protein-2 is a tumor promoter that drives cancer proliferation through its client mRNAs IGF2 and HMGA1. Elife 2017;6:e27155
23. Farahani RM, Xaymardan M. Platelet-derived growth factor receptor alpha as a marker of mesenchymal stem cells in development and stem cell biology. Stem Cells Int 2015;2015:362753
24. Shin S, Pang Y, Park J, et al. Dynamic control of adipose tissue development and adult tissue homeostasis by platelet-derived growth factor receptor alpha. Elife 2020;9:e56189
25. Clevers H, Nusse R. Wnt/β-catenin signaling and disease. Cell 2012;149:1192–1205
26. Wang X, Lu Z, Gomez A, et al. N^6-methyladenosine-dependent regulation of messenger RNA stability. Nature 2014;505:117–120
27. Edupuganti RR, Geiger S, Lindeboom RGH, et al. N^6-methyladenosine (m^6A) recruits and repels proteins to regulate mRNA homeostasis. Nat Struct Mol Biol 2017;24:870–878
28. Hafner M, Landthaler M, Burger L, et al. Transcriptome-wide identification of RNA-binding protein and microRNA target sites by PAR-CLIP. Cell 2010;141:129–141
29. Conway AE, Van Nostrand EL, Pratt GA, et al. Enhanced CLIP uncovers IMP protein-RNA targets in human pluripotent stem cells important for cell adhesion and survival. Cell Rep 2016;15:666–679
30. Hämmerle M, Gutschner T, Uckelmann H, et al. Posttranscriptional destabilization of the liver-specific long noncoding RNA HULC by the IGF2 mRNA-binding protein 1 (IGF2BP1). Hepatology 2013;58:1703–1712
31. Degrauwe N, Suvà ML, Janiszewska M, Riggi N, Stamenkovic I. IMPs: an RNA-binding protein family that provides a link between stem cell maintenance in normal development and cancer. Genes Dev 2016;30:2459–2474
32. Cao J, Mu Q, Huang H. The roles of insulin-like growth factor 2 mRNA-binding protein 2 in cancer and cancer stem cells. Stem Cells Int 2018;2018:4217259
33. Saxton RA, Sabatini DM. mTOR signaling in growth, metabolism, and disease. Cell 2017;169:361–371
34. Hara K, Yonezawa K, Weng QP, Kozlowski MT, Belham C, Avruch J. Amino acid sufficiency and mTOR regulate p70 S6 kinase and eIF-4E BP1 through a common effector mechanism. J Biol Chem 1998;273:14484–14494
35. Avruch J, Hara K, Lin Y, et al. Insulin and amino-acid regulation of mTOR signaling and kinase activity through the Rheb GTPase. Oncogene 2006;25:6361–6372
36. Oshiro N, Rapley J, Avruch J. Amino acids activate mammalian target of rapamycin (mTOR) complex 1 without changing Rag GTPase guanyl nucleotide charging. J Biol Chem 2014;289:2658–2674
37. Carnevalli LS, Masuda K, Frigerio F, et al. S6K1 plays a critical role in early adipocyte differentiation. Dev Cell 2010;18:763–774
38. Yi SA, Um SH, Lee J, et al. S6K1 phosphorylation of H2B mediates EZH2 trimethylation of H3: a determinant of early adipogenesis. Mol Cell 2016;62:443–452
39. Polak P, Cybulski N, Feige JN, Auwerx J, Rüegg MA, Hall MN. Adipose-specific knockout of raptor results in lean mice with enhanced mitochondrial respiration. Cell Metab 2008;8:399–410
40. Sabatini DM. Twenty-five years of mTOR: uncovering the link from nutrients to growth. Proc Natl Acad Sci U S A 2017;114:11818–11825
41. Bagchi DP, MacDougald OA. Wnt signaling: from mesenchymal cell fate to lipogenesis and other mature adipocyte functions. Diabetes 2021;70:1419–1430
42. Dijksterhuis JP, Petersen J, Schulte G. WNT/Frizzled signalling: receptor-ligand selectivity with focus on FZD-G protein signalling and its physiological relevance: IUPHAR review 3. Br J Pharmacol 2014;171:1195–1209
43. Gurney A, Axelrod F, Bond CJ, et al. Wnt pathway inhibition via the targeting of Frizzled receptors results in decreased growth and tumorigenicity of human tumors. Proc Natl Acad Sci U S A 2012;109:11717–11722
44. Murillo-Garzón V, Gorroño-Etxebarria I, Åkerfelt M, et al. Frizzled-8 integrates Wnt-11 and transforming growth factor-β signaling in prostate cancer. Nat Commun 2018;9:1747
45. Zeng H, Lu B, Zamponi R, et al. mTORC1 signaling suppresses Wnt/β-catenin signaling through DVL-dependent regulation of Wnt receptor FZD level. Proc Natl Acad Sci USA 2018;115:E10362–E10369
46. Prossomariti A, Piazzi G, Alquati C, Ricciardiello L. Are Wnt/β-catenin and PI3K/AKT/mTORC1 distinct pathways in colorectal cancer? Cell Mol Gastroenterol Hepatol 2020;10:491–506
47. Palsgaard J, Emanuelli B, Winnay JN, Sumara G, Karsenty G, Kahn CR. Cross-talk between insulin and Wnt signaling in preadipocytes: role of Wnt co-receptor low density lipoprotein receptor-related protein-5 (LRP5). J Biol Chem 2012;287:12016–12026